Investigating the role of *alx4a* in *mitfa* repression and iridophore fate biasing

An undergraduate project presented

By:

Melanie J. Cragan

To:

the Biology Department, Rhode Island College

April 2021

[redacted]

[redacted]

ABSTRACT

It is astounding to think that every cell of an organism arises from a single cell, the fertilized egg. The fundamental goal of developmental biology is to understand the cellular and molecular dynamics of this process. For over 100 years, researchers have used a vertebrate-specific population of embryonic cells, the neural crest, as a model for understanding fundamental processes of development such as specification, differentiation, and morphogenesis. The neural crest is a unique pluripotent population of cells that gives rise to many different cell types such as neurons, craniofacial chondrocytes, and pigment cells. Larval zebrafish, *Danio rerio*, possess three neural crest-derived pigment cells: black melanophores, shiny iridophores, and yellow xanthophores. Previous studies suggest some embryonic melanophores and iridophores arise from a bipotent precursor, but the mechanisms of lineage restriction remain unknown. As part of an ongoing CRISPR/Cas9 genetic screen, our lab found that *ALX homeobox 4a (alx4a)* knockout caused a striking reduction in iridophores. I hypothesized that *alx4a* is required to repress melanophore fate and promote iridophore fate. To continue the investigation of *alx4a*, I identified and isolated two loss of function *alx4a* alleles. I also established a protocol for high efficacy genotyping, allowing for further characterization of the *alx4a* loss of function phenotype. My investigation of iridophore development provides new insight into pigment cell specification pathways in zebrafish and may broaden our understanding of conserved pathways of pigment cell migration and differentiation in humans.

TABLE OF CONTENTS

INTRODUCTION

i. Cellular Differentiation

At the moment of fertilization, one-celled zygotes are totipotent, possessing the potential to become any cell type that their genome allows. Each round of cleavage reduces a cell's potential and brings it closer to its terminal, differentiated state. How do early embryonic cells become committed to one adult cell fate, as opposed to another? This is a question that defines the field of developmental biology, and it is the one in which we base our studies of cellular differentiation.

Throughout development, cells decrease in potential and become increasingly restricted to one specific fate. In multicellular organisms, this process of differentiation allows cells to acquire specialized phenotypes and functions, generating many diverse cell types. At a molecular level, differentiation occurs through progressive changes in gene expression orchestrated by proteins called transcription factors (TFs). TFs bind to regulatory elements within the DNA and either activate or inactivate particular genes, determining when and where a gene will be expressed and ultimately what proteins a cell will produce.

A cell is considered differentiated only if it is both *specified* and subsequently *determined*. Cells are specified when they exhibit the phenotype of their prospective fate when isolated from their *in vivo* environment. At this point, cells are still labile, meaning that their fate can be altered under the right circumstances or if they are exposed to certain signals. Cells are considered determined when fate is irreversible.

In developmental biology, there are three main modes of cell specification seen in various animal taxa. Autonomous specification occurs in many invertebrates. In autonomous specification, cells are specified to their fates early in development by maternal messenger RNAs (mRNAs) and proteins deposited in the egg cytoplasm. Early cleavage apportions these proteins and mRNAs into some cells while excluding them from others. The cytoplasmic inheritance of a transcription factor by one cell and not another sets the two cells on very different developmental trajectories. For example, in tunicates, *Macho* mRNA is restricted to a single cell at the eight-cell stage. If this cell is removed from the embryo, it autonomously develops into muscle tissue, and the remainder of the embryo doesn't make muscle (Whittaker 1973). No other cell in the embryo expresses *Macho*, and therefore no other cell can activate the expression of genes necessary for muscle development. For these reasons, *Macho* is both necessary and sufficient for muscle formation in tunicates (Nishida and Sawada 2001). This phenomenon demonstrates that maternally deposited information has positional specificity, and these determinants are crucial to the normal development of major structures.

Maternally deposited mRNAs and proteins are also the main drivers of syncytial specification, an arthropod-specific form of specification which is best studied in *Drosophila melanogaster*. In this case, the first thirteen rounds of mitosis occur without cytokinesis, but the blastoderm (blastula-stage embryo) still assigns identity to future cells with a polarized gradient of two TFs: Bicoid and Caudal (Mazumdar and Mazumdar 2002; Tomer et al. 2012). The accumulation of Bicoid to one side of the embryo results in anterior pole establishment and the accumulation of Caudal to the other side of the embryo results in posterior pole establishment. Nuclei within the syncytium experience different levels of these two transcription factors, resulting in gene expression appropriate to their location along the anterior-posterior axis. In the

context of the syncytium, gradients of Bicoid and Caudal act as morphogens, molecules that determine cell fate based on concentration.

Paracrine and juxtracrine signaling molecules also act as morphogens and are important for conditional specification in vertebrates. In conditional specification, cells achieve their fates through interactions with their neighbors. Cells receive signals produced by neighboring cells, causing a change in gene expression, ultimately specifying cells to particular fates. Here, cell-extrinsic signals must be integrated with cell-intrinsic transcription factors to achieve differentiation. Common models for vertebrate development, the African clawed frog (*Xenopus laevis)* and the zebrafish *(Danio rerio),* mainly exhibit conditional specification, although they also employ some aspects of autonomous specification. Studying the development of vertebrates is critical to understanding conserved developmental pathways and genetic disorders in humans.

ii. The Neural Crest

The vertebrate neural crest has served as a popular model for understanding cell fate specification and differentiation for over a century. Often referred to as the fourth germ layer, neural crest cells (NCCs) are a unique population of embryonic cells that have been historically referred to as "the only interesting thing about vertebrates" (quoted by P. Thorogood). Wilhelm His first observed neural crest cells in chicken embryos in 1868, calling them *Zwischenstrang*, or 'intermediate cord,' because of the way they were sandwiched between the neural tube and the epidermis. Since their discovery, developmental biologists have been fascinated by this transient population of embryonic cells.

Foundational work by Nicole Marthe Le Douariun and others used classic embryologic techniques to determine the vast diversity of adult cell types produced by the embryonic neural

crest, as well as the migratory pathways these cells use to reach their final locations (Le Douarin and Teillet 1973; Le Lièvre and Le Douarin 1975; Le Douarin 1980). The stunning diversity of cell types produced by the neural crest includes nerves and glia of the peripheral nervous system, craniofacial cartilage, bone, cells of the adrenal medulla, as well as various pigment cell types in different vertebrates (Burstyn-Cohen et al. 2004). In fact, many defining vertebrate features such as the jaws, face, skull, and bilateral sensory ganglia can be accredited to the emergence of NCCs during evolution (Davidson et al. 1998). It is astonishing that all of these adult structures arise from a single population of embryonic cells. A classic and enduring question of neural crest biology is *how* and *when* are neural crest cells restricted to specific fates?

During embryogenesis, NCCs arise along the neural plate border. After the neural plate has folded to create the neural tube, NCCs begin to delaminate from the neuroepithelium and migrate to various regions throughout the embryo (Fig. 1). At this stage, this cell population is referred to as migratory neural crest cells. As they migrate, NCCs receive signals from their tissue environment that guide them to various destinations throughout the developing embryo and promote their differentiation.

Initial specification of the neural crest occurs along the neural plate border and involves a combination of Wnt, BMP, Notch, retinoic acid, and fibroblast growth factor (FGF) signaling (Milet and Monsoro-Burq 2012). These signals work in conjunction to induce expression of a set of early neural crest-specific transcription factors, including *Snail*, *Forkhead box D3* (*Foxd3)*, and *SRY Box 9* (*Sox9)* (Theveneau and Mayor 2012). These early TFs act to promote an epithelial-mesenchymal transition (EMT), which is required for NCCs to leave the neural ectoderm and begin migration. Studies in mice have highlighted the role of one of the TFs, SNAIL, throughout this process. One study showed that SNAIL is required to represses E-

cadherins and components of adherens junctions, allowing the NCCs to detach from the neural tube and migrate independently (Cano et al. 2000). Additionally, Wnt-mediated activation of *cyclin D1*, also contributes to the transition to motility (Burstyn-Cohen et al. 2004). Once NCCs detach from the neural tube, they must migrate to their correct location within the embryo. Their point of origin along the anterior-posterior body axis plays an important role in where they will go, the path that they will take to get there, and finally, what they will become when they reach their destination.

The cranial (cephalic) neural crest originates at the most anterior end of the neural tube and migrates into the pharyngeal arches, which eventually produce structures of the developing head and neck. To enter the pharyngeal arches, cranial neural crest cells undergo collective migration to follow another cluster of cells called a placode. Placodes emit a chemoattractant *stromal cell derived factor 1* (SDF1*)*, which pulls NCCs near due to the presence of *chemokine receptor 4* (CXCR4*)*. However, when the NCCs get close enough to make contact with the placode, the placode repels away due to a contact inhibition of locomotion (CIL) response (Theveneau and Mayor 2012; Scarpa and Mayor 2016). Cranial neural crest cells ultimately differentiate as cartilage, bone, cranial neurons, glia, pigment cells, and connective tissue of the craniofacial skeleton (Calloni et al. 2009).

The cardiac neural crest forms just posterior to the cranial neural crest and can develop into melanocytes, cartilage, connective tissue, and neurons (Le Lièvre and Le Douarin 1975). These NCCs also produce connective tissue of the arteries of the heart (Sizarov et al. 2012). The vagal NCCs arise from the anterior region of the spine and give rise to enteric neurons (Le Douarin and Teillet 1973). Lastly, the trunk NCCs arise just posterior to the vagal neural crest and produce

pigment cells, nerves, and glia. Trunk neural crest cells take two different migratory pathways as they leave the dorsal neural tube, and the route they take is intricately tied to their ultimate fate.

Cells taking the ventromedial pathway travel in-between the neural tube and mesodermal tissue called somites. They then continue towards the ventral side of the embryo, where they give rise to Schwann cells and dorsal root ganglia (Serbedzija et al. 1990). In the dorsolateral pathway, NCCs travel over the somites and beneath the epidermis at the dorsal edge of the embryo. In many vertebrate species, the only neural crest cells to access the dorsolateral pathway are pigment cells called melanocytes (Erickson and Goins 1995).

Multipotency is a hallmark trait of the neural and is seen in all subpopulations. There is still some controversy over when during development NCCs become restricted to their fates, but most current models suggest a sequential process of fate restriction. In these models, the activity of both cell-intrinsic factors, like transcription factors, and extrinsic signals provided by the cellular environment, are required to promote specific fate outcomes (Raible and Eisen 1994; Henion and Weston 1997). Additionally, it has been demonstrated that some neural crest cells remain multipotent until late stages of development and that some NCCs are even capable of *de*differentiation, which is the process of going from a fate-determined cell back to a multipotent cell (Zabierowski et al. 2011).

Of the many neural crest cell derivatives, melanocytes are among the best-studied in terms of cell fate specification. Melanocytes are specified by *microphthalmia-associated transcription factor* (MITF), the master regulator of melanocyte fate (Nguyen and Arnheiter 2000). MITF is a basic helix-loop-helix leucine zipper transcription factor that promotes melanophore fate by regulating the expression of many genes involved in melanin synthesis (Hodgkinson et al. 1993). It is also sufficient to drive ectopic melanophore development (Tachibana et al. 1996). *Mitf*

expression is directly activated by Wnt binding to its promoter regions (Dorsky et al. 1998). Utilization of the trunk dorsolateral pathway during NCC migration is reserved for cells specified as melanocytes. Historically, developmental biologists have studied the processes of neural crest specification and morphogenesis in chickens, mice, and amphibians, but more recently, they have turned to the zebrafish (*Danio rerio*).

iii. *Danio rerio* as a Model System in Developmental Biology Studies

Zebrafish (*D. rerio)* are native to South Asia and are frequently sold in pet stores under the name "Danios." As adults, they are 3-4 cm in length, and as one might infer, they possess distinct horizontal stripes. Zebrafish are now commonly used as biomedical research organisms. Their rapid development, controllable spawning, easy maintenance, and fully sequenced genome make them an attractive system for studying diverse topics, including fin regeneration, gene expression, pharmacology, physiology, environmental toxicology, and cancer biology.

Unlike mammals which only have melanocytes, zebrafish have three different neural-crest derived pigment cells. Black melanophores produce melanin and are homologous to mammalian melanocytes, while iridescent iridophores contain stacks of reflective purine platelets, and yellow xanthophores contain pteridines (Fig. 2). These chromatophores are organized to produce distinct early larval, mid-larval, and adult pigment patterns. The early larval (EL) pattern consists of dorsal and ventral stripes made of melanophores and iridophores, as well as a lateral stripe made of only melanophores. Xanthophores are concentrated dorsally, giving the organism an overall faint yellow appearance. Chromatophore precursors migrate directly from the neural crest to their position within the early larval pattern, but the different cell types take different migratory pathways to get there. Presumptive iridophores migrate ventromedially, xanthophores migrate

dorsolaterally, and melanophores utilize both pathways. Pigment cells reach their final positions within the early larval pattern by 3 days post-fertilization (3 dpf). Around 14 dpf, this early larval pattern is replaced by newly differentiated adult pigment cells, which will produce the characteristic striped pattern of the adult (Kelsh et al. 2009). In zebrafish, the guidance signals which direct presumptive chromatophores from the neural crest to their positions within the EL pattern are not well known. Additionally, it is not yet clear how pigment cells are specified to their fates.

iv. Pigment cells and gene regulatory networks in *D. rerio*

One way to understand how neural crest cells are specified to particular chromatophore lineages is by studying gene regulatory networks (GRNs). These networks map the inhibition and activation of different genes by TFs within a cell, which shows how variation of transcription levels accounts for cell function. GRNs are often used in developmental biology to model lineage restriction and differentiation (Martik et al. 2016; Buckingham 2017).

One of the best-studied neural crest gene regulatory networks in zebrafish is that of the melanophore. *Melanocyte Inducing Transcription Factor* (*Mitf)* is the master regulator of melanophore fate and has been found to repress the fates of other pigment cells in a multitude of species (Hallsson et al. 2007). The activity of zebrafish *mitfa* has been described with experimental data and mathematical modeling (Greenhill et al. 2011). For example, the model details the relationship between *mitfa* and *SRY-Box transcription factor 10* (*sox10)*, one of the early neural crest TFs. During melanophore differentiation, *sox10* is downregulated so that *mitfa* and other melanocyte-specific genes can be expressed (Greenhill et al. 2011).

Several studies suggest that early larval melanophores and iridophores arise from bipotent precursor cells. It is hypothesized that various transcription factors are needed to repress melanophore fate and bias these cells towards an iridophore fate and vice versa. Previous studies suggest that *Foxd3* represses *mitfa* and consequently melanophore differentiation (Curran et al. 2009; Curran et al. 2010). *Foxd3* is expressed in iridophore and xanthophore precursory cells, which demonstrates that it biases cells away from a melanophore fate and towards other chromatophore fates. Zebrafish *foxd3* mutants have higher *mitfa* expression in the head and anterior region, but they don't have significantly more melanophores (Curran et al. 2009). Although *Foxd3* represses *mitfa*, the absence of the *foxd3* gene does not result in an increase in melanophores. This result suggests that additional genes are likely needed to repress melanophore fate in zebrafish.

Two proteins: *transcription factor EC (tfec)* and *leukocyte receptor tyrosine kinase (ltk),* have been found to work in concert in the iridophore GRN to promote iridophore fate. *Tfec*, a transcription factor, is expressed in zebrafish NCCs as early as 18 hpf. *Ltk,* a transmembrane receptor protein, is expressed in the late presumptive chromatophore (chromatoblast) stage, which begins around 22 hpf (Petratou et al. 2018; Petratou et al. 2021). Both proteins promote iridophore fate via a positive feedback loop, which functions to upregulate the expression of the iridophore differentiation genes including, *purine nucleoside phosphorylase 4a* (*pnp4a).* However, iridophore GRN modeling using known genes is insufficient to account for repression of *mitfa*, and ultimately melanophore fate (Petratou et al. 2018). This prompted the introduction of a "Factor R" to fill this void in the iridophore GRN. Factor R is predicted to repress *mitfa* and promote *pnp4a* (Petratou et al. 2018). In other words, a cell can only be specified as an

iridophore if Factor R is expressed and *mitfa* is repressed. The identity of Factor R, a significant element of the iridophore GRN, remains a tantalizing unknown.

v. *ALX homeobox* genes

Aristaless-like homeobox (Alx) genes are homeobox transcription factors belonging to the PRD (Paired-like) gene family, which includes well-known genes like *Orthodenticle Homeobox (Otx)* and the *Paired Box* (*Pax)* paralogs. In humans and mice, ALX genes are known to play roles in neural tube closure, limb development, and craniofacial development (Zhao et al. 1996; Qu et al. 1997). The mouse ortholog, *Alx-4,* is expressed in neural crest cells undergoing EMT during development (Hudson et al. 1998). Recently, RNA-seq transcriptomic analysis revealed that ALX-3 was upregulated in light stripes relative to dark stripes in African striped mice. *Alx-3* overexpression reduces *Mitf* expression as a result of direct binding of ALX-3 to the promoter region in the *Mitf* gene (Mallarino et al. 2016). Additionally, in zebrafish, loss of function (LOF) mutations in *alx-1* result in frontonasal dysplasia (Dee et al. 2013). These are key indications that ALX genes play important roles in neural crest migration.

Recently, transcriptome profiling of thousands of neural crest-derived cells was conducted in zebrafish, and two *alx* genes, *alx4a* and *alx4b,* were found to be expressed by iridophores but not by melanophores at 5 dpf (Saunders et al. 2019). Given the known roles of other *Alx* genes in neural crest development, expression of *alx4a* and *alx4b* by iridophores is intriguing, and these genes are good candidates for Factor R, the hypothesized repressor of melanophore fate in zebrafish. Currently, there are no known *alx4a* or *alx4b* mutants in zebrafish and *alx homeobox 4* genes have never been studied in the context of pigment cell development.

vi. CRISPR/Cas9 knockout of *alx4a*

Clustered regularly interspaced short palindromic repeats, or "CRISPR" are DNA sequences within prokaryotes that reflect fragments of phages that previously invaded their species. As an immune response, bacteria produce a protein called Cas9 when being invaded by a bacteriophage. In an attempt to eradicate the phage, Cas9 induces double-stranded breaks in the phage DNA. Recently, scientists have harnessed this innate biological ability to induce double-stranded breaks in targeted DNA (Jinek et al. 2012).

CRISPR/Cas9 is an efficient method for generating mutations in a gene of interest. This technique works by inducing a double-stranded break in the DNA and then allowing the cell to repair the damage with non-homologous end joining (NHEJ) (Fig. 3). NHEJ is an imperfect cellular repair system and often results in lost nucleotides and consequently missense or nonsense mutations. This system allows for the potential introduction of premature stop codons into genes of interest, thus knocking out the function of an associated protein. Noticeable phenotypes in the mutant suggest that the mutagenized gene may play a role in the normal development of the phenotype. Recently, biologists have been using *D. rerio* as a model for CRISPR genetic screening. Embryos are relatively large, stages of cleavage are distinguishable, and development occurs predictably (Fig. 4). These factors make it easy to perform CRISPR/Cas9 microinjections and analyze phenotypes in zebrafish.

vii. The Role of *alx4a* in Iridophore Development

The goal of this project was to investigate the role of *alx4a* in promoting iridophore fate from a bipotent precursor. I hypothesized that *alx4a* is required for iridophore fate specification and that it also represses *mitfa* expression. I used CRISPR/Cas9 to knockout *alx4a* in zebrafish

embryos. I discovered that knockout of *alx4a* produced larvae with severely decreased iridophores, suggesting that *alx4a* qualifies as a candidate for Factor R. To further investigate the role of *alx4a* in iridophore specification, I identified two loss of function *alx4a* alleles, isolated homozygous mutant lines of both alleles, and confirmed the loss of iridophores in *alx4a* homozygous mutants. Together, these data demonstrate the necessity of *alx4a* for iridophore development in zebrafish. The current investigation of *alx4a* may help to identify a key factor in the iridophore GRN and explain how bipotent precursory cells become biased towards an iridophore fate.

METHODS

Ethics Statement

All animal research was conducted according to federal, state and institutional guidelines and in accordance with protocols approved by the Institutional Animal Care and Use Committee at Rhode Island College. Anesthesia and euthanasia were performed using MS-222.

Fish Stocks and Rearing Conditions

All zebrafish stocks were generously provided by David M. Parichy (University of Virginia). Stocks include: *mitfa-egfp* (Curran et al. 2009), *NHGRI-1* (LaFave et al. 2014), *pnp4a-egfp* (Spiewak et al. 2018) and $kita^{b5}$ (Parichy et al. 1999). New stocks $alx4a^{ex1+8}$ and $alx4a^{ex1-4}$ were generated as part of this study. Fish were reared at standard conditions (14L:10D light cycle, 28.5°C) and fed marine rotifers, brine shrimp, and flake food. They were spawned naturally, or gametes were harvested for *in vitro* fertilization (IVF). Embryos were placed in 10% Hanks medium and incubated at 28.5°C.

CRISPR/Cas9 knockout of *alx4a*

Guide RNAs targeting *alx4a* in *D. rerio* were designed using CHOPCHOP (Labun et al. 2019). The target sequence 5'-GAAAACAGCGGACACAACGG-3' was chosen for its high predicted efficiency, GC content, and a 0 for self-complementarity rate.

Overlap PCR was used to generate a DNA template for gRNA synthesis. In this procedure, a scaffold oligo with a binding site for T7 RNA polymerases is annealed to an oligo carrying the *alx4a* target site using Q5 DNA polymerase (NEB) and the following cycling conditions: 98°C

10s, [98°C 5s, 55°C 15s] 32X, 72°C 60s, 4°C hold. PCR products were run on a 2% agarose gel with SYBR Safe DNA gel stain. Successful PCR products were purified with Zymo Clean and Concentrate kits (Zymo Research). A transcription reaction was performed using with 1.5 µl each of 10X buffer, ATP, CTP, GTP, UTP, and T7 Polymerase with 650ng of the purified PCR. Transcription reactions were incubated at 37°C overnight. RNA was precipitated using LiCl and resuspended in nuclease-free H_2O. Purified gRNAs were stored at -80°C.

Prior to microinjection, gRNAs were diluted to 200 ng/µl. An injection solution including 1 µl of 1000 ng/µl Cas9 protein (PNA Bio), 1 µl of 200 ng/µl gRNA and 1 µl of Fast Green dye was prepared prior to injection. This solution was incubated on ice for 10 minutes to allow association between Cas9 protein and *alx4a* targeting gRNAs. The injection solution was injected into 1-cell embryos from *mitfa-egfp* x *kit*^{b5} crosses using a Picrospritzer (Parker Hannifin) according to standard protocols (Shah et al. 2015).

Genomic DNA isolation, PCR and sequencing

I. Genomic DNA extraction

At 24 hpf, genomic DNA (gDNA) was isolated from pools of four F0 injected embryos by following standard hot base gDNA extraction protocol (Shah et al. 2015). To genotype adult individuals, fin clipping was performed followed by hot base gDNA extraction (Xing et al. 2014).

II. *alx4a* Amplification and Sequencing

PCR was performed to verify Cas9 mutagenesis of *alx4a* using Q5 polymerase and following standard protocols (Shah et al. 2015). Forward primer 5'- GGCACCTTTAACAAATACCACC-3' and reverse primer 5'- CAGTCATAAAAACGCGAATGTC-3' were used to generate an

amplicon of 268 base pairs (bp) surrounding the *alx4a* gRNA target site. Cycles were run with an annealing temperature of 63°C. Products were run on a 2% agarose gel. Samples of interest were purified with Zymo Clean and Concentrate Kit (Zymo Research) and set up for sequencing according to the Sanger Sequencing protocol from the University of Rhode Island (URI). Sequences were analyzed using CLC Main Workbench 20 (https://digitalinsights.qiagen.com).

pJET Cloning and Plasmid Sequencing

I. pJET Ligation and Transformation

Prior to ligation, pure PCR products were diluted to 10ng/ul. It was then added to a ligation reaction using the CloneJET PCR cloning kit and pJET1.2/blunt vector (Thermo Fisher Scientific). The recombinant plasmids were then used in a transformation reaction performed with DH10B competent cells (Thermo Fisher Scientific). The following protocol was used: 2 µl of the ligation mix was added to 25 µl competent cells. Cells were placed on ice for 30 minutes, followed by a 30 second heat shock at 42°C. for 30 seconds. After a 2-minute recovery on ice, 250 µl SOC Outgrowth Medium was added to the cells, and they were placed in a 37°C shaking incubator for 60 minutes at 250 rpm.

II. Cell Plating and Cultures

Transformations were plated onto LB+AMP plates and incubated at 37°C overnight. Approximately 24 hours after plating, individual colonies were picked and placed in 2ml of LB broth +AMP (1 µl AMP/ml LB broth) in culture tubes. Cultures were then placed in the 37°C shaker overnight.

III. Plasmid Minipreps

Plasmids were isolated from overnight cultures using the Monarch Plasmid Miniprep Kit and following manufacture's protocol (NEB). Plasmids were then amplified with PCR to verify insert using forward primer: 5'-CGACTCACTATAGGGAGAGCGGC-3' and reverse primer 5'-AAGAACATCGATTTTCCATGGCAG-3'. Products were run on a 2% agarose gel. Plasmids with successful PCR products were diluted to 200 ng/µl and set up for Sanger Sequencing according to protocol given by the University of Rhode Island. Sequencing reactions were analyzed using the same protocol as above stated.

Genotyping protocol for *alx4a*$^{ex1+8}$.

F0 Cas9 injected embryos were grown to adult stages and outcrossed to wild-type individuals. F1 progeny were then intercrossed, producing a population of F2 individuals which, according to Mendelian genetics, contain wild-type homozygotes, heterozygotes, and *alx4a* mutant homozygotes. Following fin clipping and gDNA extraction, PCR was performed using forward primer: 5'- TATCTGTTCGCTTTGCTCTCCA-3' and reverse primer: 5'-CCTCGCGGCATATTTCATGTTT-3'. Annealing temperature was set to 67°C, and extension time was set to 45s. Successful amplification was confirmed by gel electrophoresis. PCR products were incubated at 37°C for 5 hours with restriction enzyme Hpy188i (New England Biolabs, USA), which cut mutant *alx4a*$^{ex1+8}$ allele into fragments of 460 and 412 bp. Digest reactions were run on a 2% agarose gel and imaged with Bio-Rad imager to confirm genotypes.

Imaging and image analysis

All microscopy was done with a Zeiss Axiozoom v.16 equipped with a Zeiss Axiocam 506 color camera, or a Zeiss Discovery v.8 equipped with an Axiocam 503 color camera.

F0 injected embryos and uninjected controls were imaged at 3 and 5 dpf.

Heterozygous carriers of *alx4a* mutations were outcrossed to the iridophore specific transgenic line *pnp4a:GFP*. Prior to imaging, all larvae were anesthetized with Tricaine and placed in methylcellulose for immobilization. Individuals were imaged with a Zeiss stereoscope both in brightfield and epifluorescence to visualize GFP. Individuals carrying the transgene were confirmed by the presence of GFP presence in the retina and genotypes were verified by Hpy188i genotyping (described above). FIJI image analysis software was used to quantify the area of the eyes as well as that of the iridophore coverage of the eyes in wild-type and *alx4a* mutant individuals.

RESULTS

F0 knockouts of *alx4a* developed few iridophores

To test the role of *alx4a* in promoting iridophore fate in zebrafish, I used CRISPR/Cas9 to knock out *alx4a*. Guide RNAs targeting exon1 of *alx4a* were injected along with Cas9 protein into 1-2 cell embryos (Fig. 4). Cas9 introduces a double-stranded break in the DNA, which is repaired via non-homologous end joining (NHEJ), an intrinsic cellular process (Fig 3). Compared to wild-type siblings, 3 dpf F0 *alx4a* knockouts developed far fewer iridophores (Fig. 5). Sanger sequencing results verified that CRISPR/Cas9 microinjections did generate mutations in exon 1 of *alx4a* in F0 injected embryos.

Identification and Isolation of *alx4a* loss of function alleles

F0 CRISPR/Cas9 injections produce mosaic phenotypes because some cells retain the wild-type *alx4a* allele while others carry mutated versions. Additionally, due to the high incidence of biallelic mutations induced by CRISPR/Cas9, individuals may have multiple *alx4a* alleles (Cong et al. 2013; Dow et al. 2015). This can make it challenging to interpret phenotypes in the F0 generation. To better understand the role of *alx4a* in iridophore fate specification, I sought to isolate lines of loss of function *alx4a* alleles. F0 *alx4a* knockouts that developed few iridophores were grown to adult stages and then outcrossed to wild-type fish to produce an F1 generation. The individuals of the F1 generation were potentially heterozygous carriers of *alx4a* mutations (Fig. 6). All F1 individuals were phenotypically wild-type, suggesting *alx4a* mutant alleles are recessive. The F1 generation was then intercrossed with the goal of recovering the original F0 phenotype. To identify specific *alx4a* mutant alleles, genomic DNA was extracted from F2 individuals with few or no iridophores (Fig. 6). PCR was used to amplify the genomic

region surrounding the *alx4a* gRNA target and then cloned into a pJET plasmid and sequenced. Sequence analysis identified two distinct *alx4a* alleles in exon 1: an 8 bp insertion and a 4 bp deletion (Figs. 7A-B). Both alleles were isolated from the F1 progeny of a single F0 injected female (Fig. 6). Both mutations likely represent loss of function alleles since they generate premature stop codons upstream of the DNA binding homeobox domains (Fig. 7C). The 8 bp insertion also introduced a binding site recognized by the restriction enzyme Hpy188i (Fig. 7B). This allowed me to distinguish between wild-type, heterozygotes, and homozygous mutants.

Using this restriction digest, I genotyped the adult F1 generation to identify carriers of the 8 bp insertion, $alx4a^{ex1+8}$ allele. Individuals which did *not* carry the 8 bp insertion were presumed to be carriers of the 4 bp deletion. Identified carriers of $alx4a^{ex1+8}$ were then intercrossed. This cross produced progeny with two distinct phenotypes. Approximately ¾ of the progeny (8/10) developed iridophores and approximately ¼ of the progeny (2/10) had no body iridophores at 3 dpf (Fig. 8A). Presumptive carriers of the 4 bp deletion allele were intercrossed and yielded similar results (Fig. 8B). Trans-heterozygous crosses ($alx4a^{ex1-4}$ x $alx4a^{ex1+8}$) also yielded similar results (Fig. 8C). These results are consistent with the expectations of Mendelian inheritance of a recessive allele (Fig. 8). Homozygous *alx4a* mutants of both alleles are semi-viable. Mutants fail to inflate their swim bladders, making it difficult to raise them to adult stages. However, I have maintained two individuals to adulthood and the iridophore deficiency persists in the adult pigment pattern (Fig. 9). These results suggest that *alx4a* is required for iridophore specification from a bipotent precursor and that no iridophores develop in the absence of alx4a.nThe protocol used to verify the presence of the $alx4a^{ex1+8}$ allele is an efficient and replicable protocol. It is a rapid method of verifying phenotype with a genotype (Fig. 10A-C)

Absence of Iridophores in *alx4a* mutants Confirmed with Iridophore Marker *pnp4a*

The apparent lack of iridophores in *alx4a* mutants could occur because no iridophores are specified in the absence of alx4a. Alternatively, iridophores could be present in the mutant but not visible because they do not produce the purine platelets that give iridophore their shiny appearance. To distinguish between these alternatives, carriers of $alx4a^{ex1+8}$ were crossed to *pnp4a:egfp,* a transgenic line in which the *pnp4a* promoter drives enhanced green fluorescent protein (EGFP) in differentiated iridophores. Individuals that inherited the transgene and $alx4a^{ex1+8}$ were intercrossed, and their progeny were analyzed for transgene expression at 4 dpf. Larvae with iridophores had EGFP expression in cells along both the dorsal (Fig. 11) and ventral sides of the body (data not shown). Larvae without iridophores had no EGFP expression along the dorsal or ventral sides of the body (Fig. 11). Hpy188i genotyping confirmed that iridophore-deficient larvae were homozygous *alx4a* mutants, and the larvae with iridophores were either heterozygous or homozygous wild-type. I was able to confirm that larvae with no body iridophores did inherit the *pnp4a-egfp* transgene because iridophores and EGFP were present in the eyes (Fig. 12A-B). Together, the results of this experiment further support the hypothesis that *alx4a* is required for an early step of iridophore differentiation.

***Alx4a* retinal ocular iridophore quantification**

I next asked whether eye iridophores were reduced in *alx4a* mutants compared to phenotypically wild-type siblings. Because it is difficult to distinguish individual iridophores in the eyes, FIJI image analysis software was used to quantify the percent of the eye covered by iridophores in wild-type ($alx4a^{+/+}$ and $alx4a^{ex1+8}/+$) and $alx4a^{-/-}$ mutants. There was no significant difference in the area of the eye covered by iridophores between *alx4a* mutants and

their wild-type siblings ($t(3)= -0.673$, $p=0.542$) (Fig. 12A, C). This result suggests that while the iridophores that produce the larval pigment pattern require alx4a for specification and differentiation, eye iridophores do not.

DISCUSSION

In this study, I sought to test the hypothesis that *alx4a* is required for iridophore fate specification in zebrafish. To do so, I isolated two different *alx4a* loss of function (LOF) alleles, established a high-efficacy system for genotyping for one of these alleles, and verified the absence of body iridophores in *alx4a* mutants using an iridophore specific reporter line. The CRISPR knockout and homozygous mutant isolation assays showed that without *alx4a*, body iridophores do not develop. This result suggests that *alx4a* is required to bias bipotent precursory pigment cells towards an iridophore fate.

By establishing a line of *alx4a+/-;pnp4a:egfp* fish, I was able to compare iridophore expression in *alx4a* heterozygotes and their homozygous mutant siblings. Using *pnp4a* as an iridophore marker, I confirmed the lack of iridophores in the mutant *alx4a* larvae. This finding also shows that alx4a is needed to drive *pnp4a* expression. If there had been EGFP expression in the mutants, I might have concluded that *alx4a* is involved in pigment synthesis as opposed to iridophore specification. Interestingly, the *alx4a* mutants showed *pnp4a:egfp* expression in the retinal pigment epithelium (RPE), and there was no significant difference between the area of the eye covered by iridophores in wild-type and mutant individuals. This finding suggests that ocular iridophores develop through a different molecular mechanism than body iridophores and that they do not require *alx4a*.

A similar result has been observed for melanophores. Although zebrafish *mitfa* mutants lack all body melanophores, they retain eye pigmentation (Lane and Lister 2012). Although *mitfa* is expressed in the retinal pigment epithelium (RPE), a different transcription factor, *Otx* is necessary for pigmentation of the RPE. Melanin-producing cells of the RPE are not neural crest-derived. The embryonic origin of reflective cells in the eye is not known, but my results suggest

that their specification and differentiation differs from the neural-crest derived iridophores that produce the larval pigment pattern.

The *alx4a* loss of function phenotype is similar to loss of function phenotypes observed for two other genes: *transcription factor EC (tfec)* and *leukocyte receptor tyrosine kinase (ltk).* Mutants for *ltk* are deficient of iridophores as well as iridoblasts, the presumptive iridophores (Lopes et al. 2008). Mutants for *tfec,* a transcription factor, are also iridophore deficient, and *tfec* is repressed by *Mitfa* in mature melanocytes (Petratou et al. 2021). In both *tfec* and *ltk* mutants, there is no alteration in dorsal melanophores along the trunk. However, in *tfec* mutants, there are significantly more melanophores on the head. Both *tfec* and *ltk* are known to be involved in the iridophore specification GRN by participating in a positive feedback loop that promotes iridophore fate (Petratou et al. 2018). However, neither of these studies have demonstrated that these proteins are able to repress *mitfa*, which is a key property of Factor R. Interestingly, both *tfec* and *ltk* mutants have a significant reduction in iridophores in the RPE. This suggests that Alx4a functions differently than Tfec and Ltk during iridophore development. The role of *alx4a* may be analogous to the activity of mitfa in melanocyte specification because *mitfa* mutants also don't show reduced pigmentation of the RPE.

It has been suggested that unidentified repressors of *mitfa* in zebrafish are required for iridophore fate specification (Curran et al. 2009). It is possible that alx4a represses *mitfa* expression, effectively blocking melanophore fate. In mice, ALX3 is able to bind and directly repress MITF (Dee et al. 2013). This study demonstrated the capacity for *Alx* genes to act as repressors of melanophore fate. To investigate the potential role of Alx4a in *mitfa* expression, we must evaluate melanophore numbers and *mitfa* expression in the *alx4a* loss of function mutants. To do so, other lab members are conducting melanophore quantification and qRT-PCR to

evaluate expression levels of *mitfa* in the mutant embryos. So far these analyses suggest that there is no obvious increase in melanophores in *alx4a* mutants at 5 dpf as might be expected if Alx4a represses *mitfa* and melanophore fate (unpublished data, C. Rei-Mohammed). This could suggest that Alx4a does not play a direct role in repression or that other proteins are able to compensate for the loss of Alx4a.

Zebrafish have two *alx4* homologs, *alx4a* and *alx4b*. It has been found that some paralogs can act in a compensatory manner for one another. For example, knockdown of *protocadherin10a* (*pcdh10a)* in zebrafish results in abnormal migration of melanophores, as well as precocious differentiation (Williams et al. 2018). In the knockdowns, *protocadherin10b (pcdh10b)* is overexpressed and the phenotype is partially restored. Only in *pcdh10a/b* double mutants is there a complete loss of normal melanophore migration. Like *alx4a*, *alx4b* is expressed in differentiated iridophores (Saunders et al. 2019). Compensatory expression could be the case for *alx4a* and *alx4b*, so it is worth investigating *alx4b* transcription in *alx4a* mutants as well as the phenotype of double mutants. We are currently working to isolate lines of *alx4b* mutant alleles to test this hypothesis.

Our preliminary work on *alx4a* provides a proof of concept for continuous investigation of the function of *alx4* genes in zebrafish pigment pattern development. Further investigation will include injections to misexpress *alx4a* and test for sufficiency for iridophore differentiation. If *alx4a* represses melanophore fate, this research will present evidence that it is the missing puzzle piece of the iridophore GRN, "Factor R," in zebrafish. Identification of Factor R will be a major step towards identifying regulators of *Mitfa* expression. Alterations of MITF expression occur during metastatic melanoma, so information regarding the regulation of MITF expression

and in particular, the identification of MITF repressors may be useful in emerging biomedical gene therapies.

FIGURES

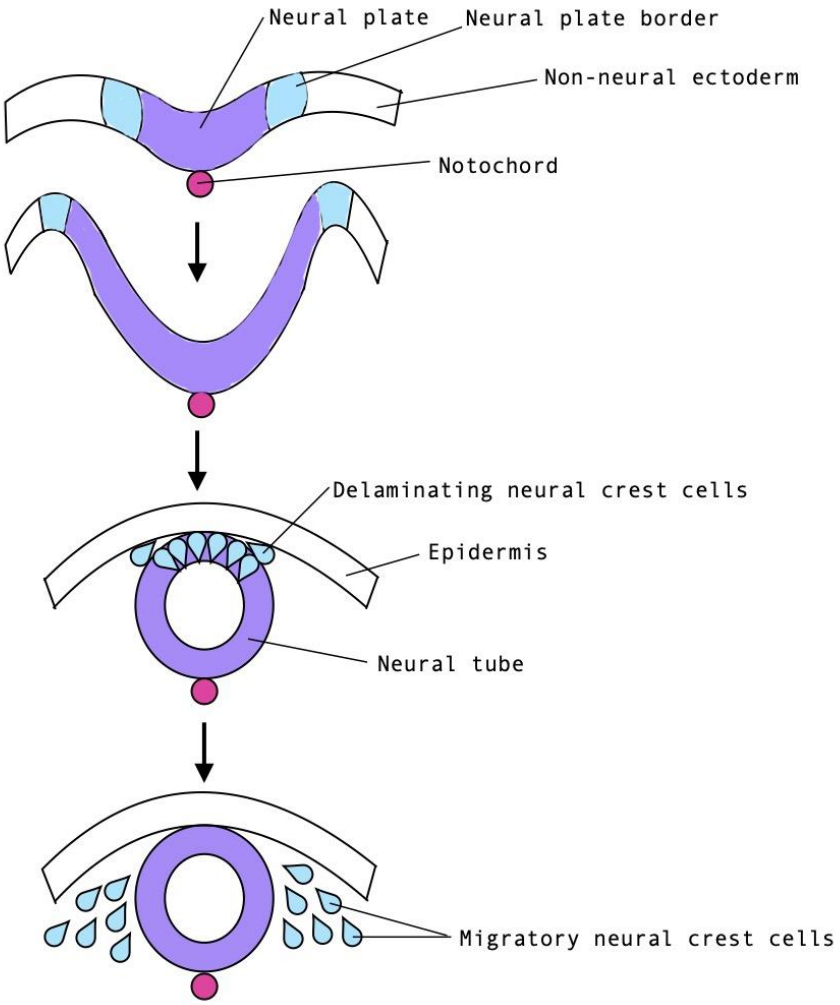

Figure 1: The neural crest cell are specified and then undergo EMT, travelling to various locations throughout the embryo.
During neural tube closure, the neural plate border cells are located between the non-neural ectoderm and the neural ectoderm. When the neural tube is fully closed, the neural plate border cells are situated at the dorsal-most point of the tube. At this point, they are referred to as the neural crest. They then undergo epithelial mesenchymal transition (EMT), which makes them motile. Diagram inspired by a figure in Developmental Biology 11th Edition, Gilbert and Barresi.

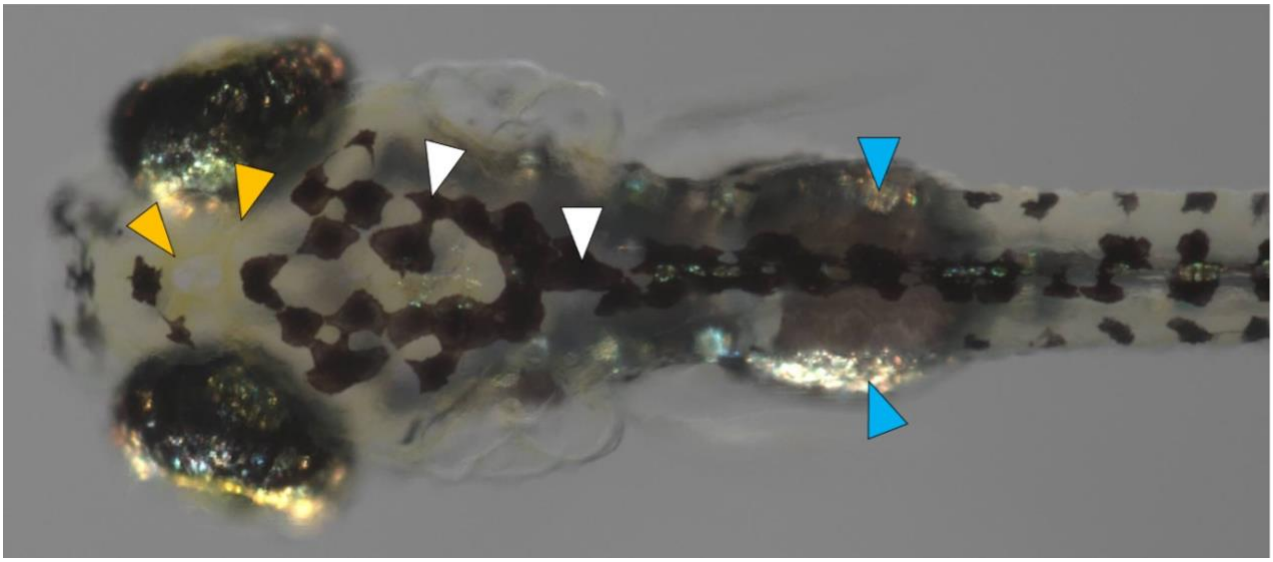

Figure 2: Three pigment cell types produce zebrafish larval pigment pattern.
A dorsal view of a 5 dpf zebrafish larva. Yellow arrowheads show xanthophores, yellow pigment cells which produce pteridine pigment compounds. White arrowheads show melanophores, black pigment cells which produce melanin pigment compounds. Blue arrowheads indicate iridophores, iridescent pigment cells which acquire their reflective properties from purine platelets.

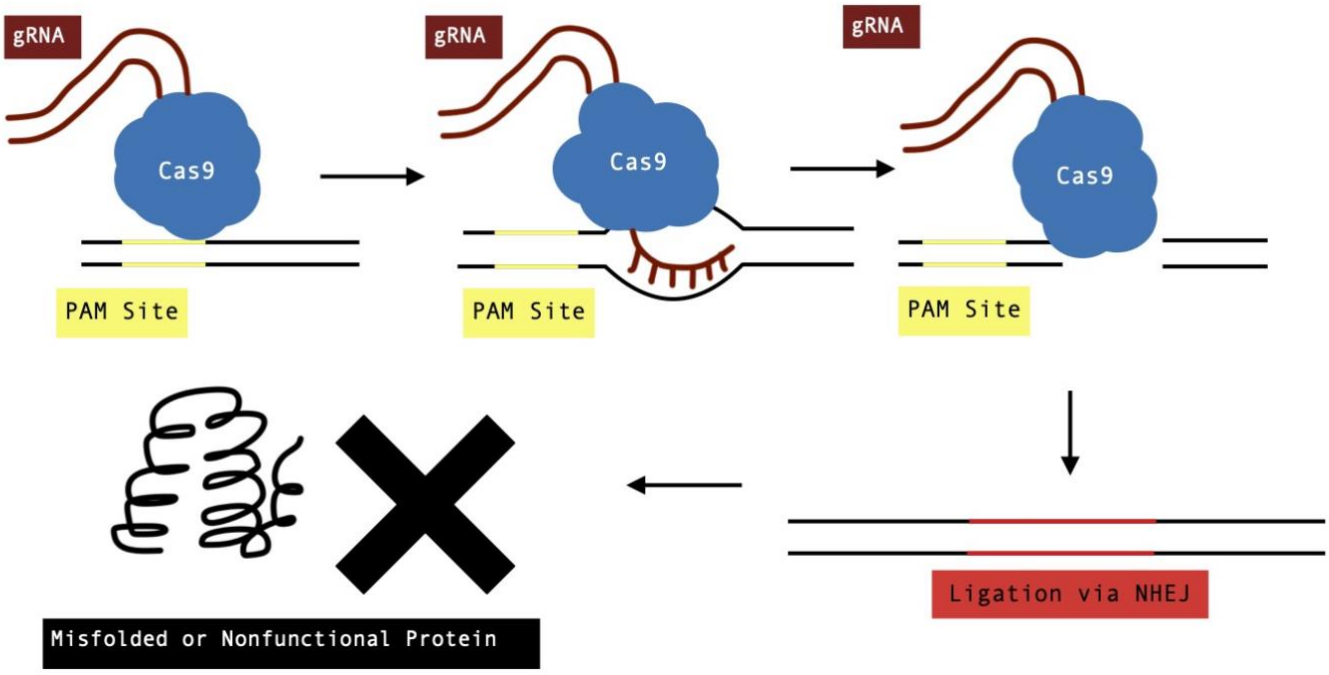

Figure 3: CRISPR/Cas9 introduces mutations via double stranded breaks which are repaired by NHEJ
Cas9 protein in association with a guide RNA (gRNA) scans DNA for PAM sites (NGG). Once found, Cas9 moves 3-4 nucleotides downstream and unzips the helix. If the complementary sequence for the gRNA is present, Cas9 makes a double stranded break in the DNA. If the target sequence is not present, the helix re-zips and the Cas9 complex keeps scanning the DNA. Following DNA damage, the cell uses non-homologous end joining (NHEJ) to repair double-strand breaks Because this is an error-prone method of DNA repair, small insertion or deletions are frequently produced as a result.

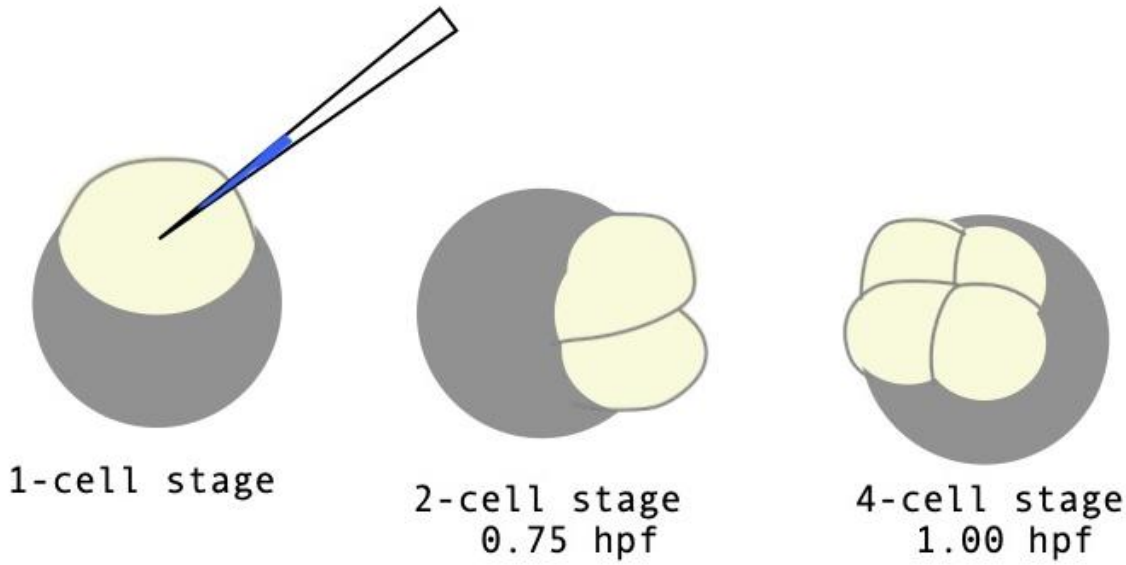

Figure 4: Cas9-gRNA complex is injected at the 1-cell stage
Zebrafish embryos undergo discoidal meroblastic cleavage. The first cleavage occurs at about 0.75 hpf. The second cleavage occurs at about 1.00 hpf, resulting in a 4-cell stage embryo. Microinjections of *alx4a* targeting gRNA and Cas9 protein were performed within one hour of fertilization.

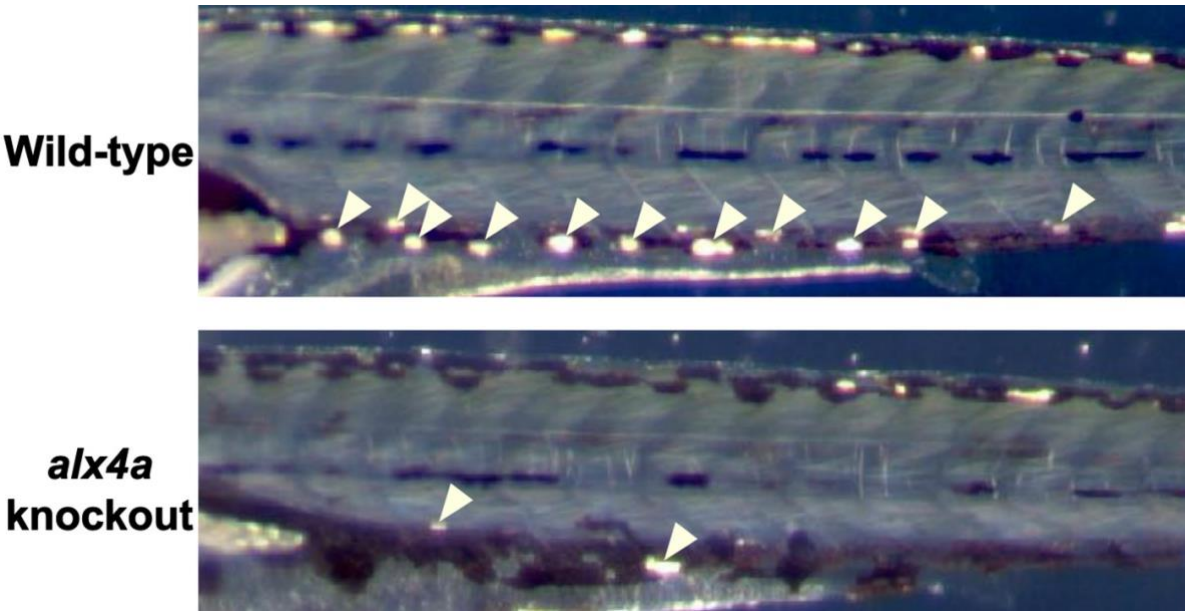

Figure 5: F0 CRISPR/Cas9 knockout of *alx4a* reduced iridophores in the ventral stripe of injected embryos
Lateral images of 3 dpf wild-type embryo (top) and embryo injected with Cas9 and gRNA targeting *alx4a* (bottom). White arrowheads show iridophores in the wild-type and CRISPR *alx4a* mutants.

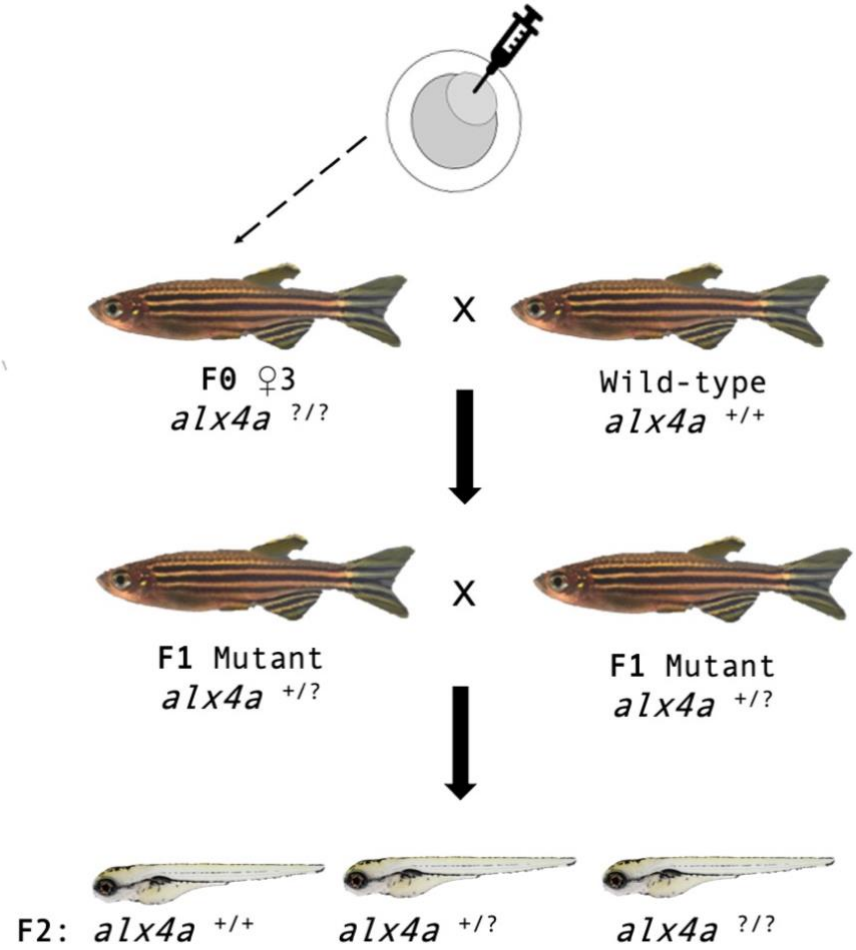

Figure 6: Breeding scheme used to identify CRISPR/Cas9 induced mutations in *alx4a*
The F0 generation was produced by injecting 1-cell zebrafish embryos with *alx4a* targeting gRNAs and Cas9 protein. Larvae with few iridophores were reared to breeding age and outcrossed to wild-type. Their progeny (F1 generation) were phenotypically wild-type (striped) but may be carriers of *alx4a* mutations. F1 fish were intercrossed to produce an F2 generation. The F2 generation displayed a range of iridophore phenotypes. Genomic DNA was extracted from individuals with few or no iridophores to identify specific lesions in *alx4a*.

Figure 7: Identification of CRISPR/Cas9 induced *alx4a* loss of function alleles
(A) Zebrafish *alx4a* gene structure. Black rectangles indicate coding exons, black lines are introns. Green indicates the region coding for the DNA binding homeobox domain. (B) Nucleotide sequences of *alx4a* exon 1 surrounding the region targeted by the *alx4a* gRNA (underlined in wild-type). Progeny from F0 female 3 had two different lesions in *alx4a*: a 4 bp deletion and an 8 bp insertion. The 8 bp insertion produces a binding site for the restriction enzyme Hpy188i (green box). (C) Amino acid sequence showing the stop codons in these alleles. Stars indicate stop codons. Red text indicates discrepancies between the mutant and wild-type amino acids.

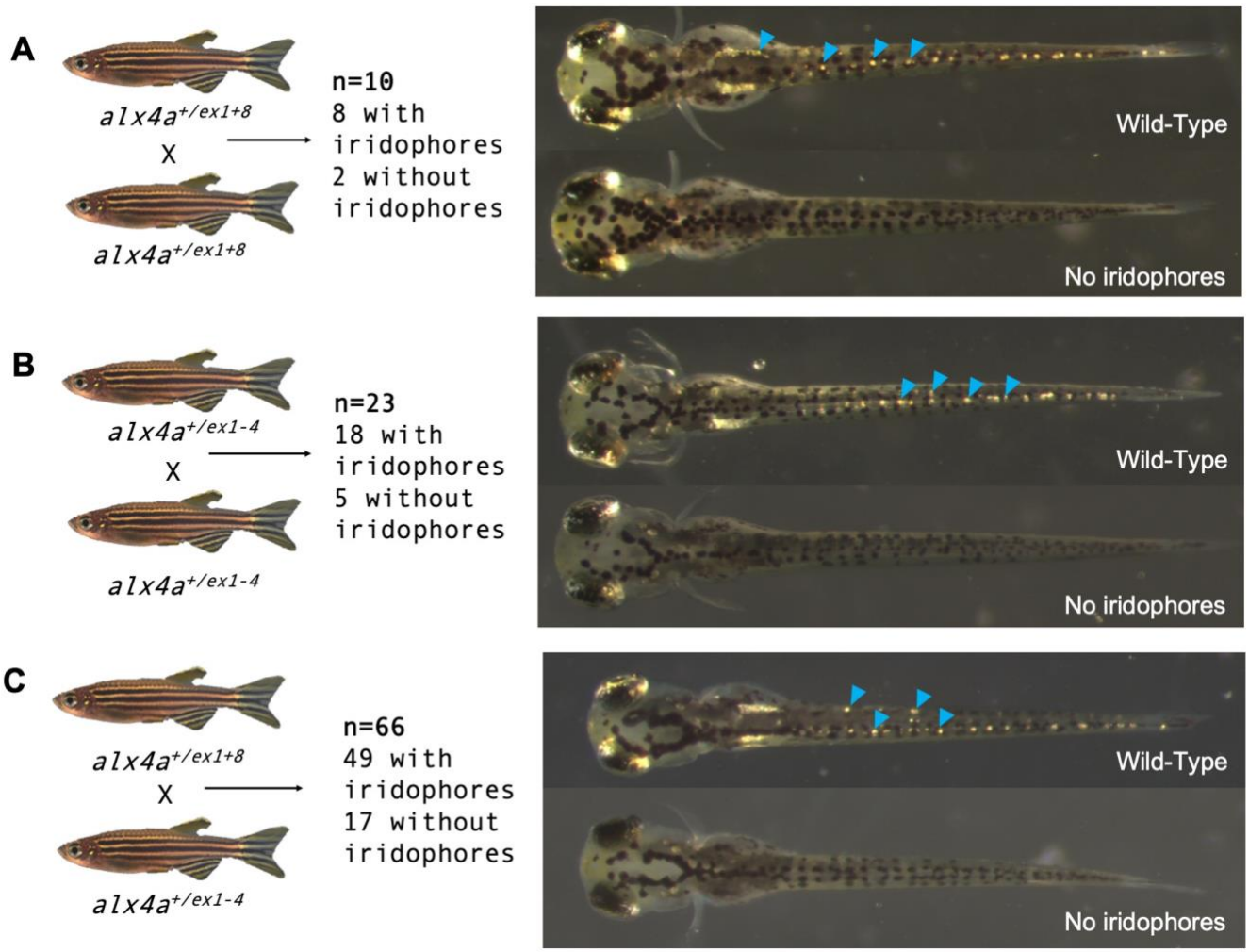

Figure 8: *alx4a* inheritance follows inheritance patterns predicted by Mendelian genetics. The expected phenotypic ratio of crosses between heterozygous carriers of recessive alleles is 3:1 (with iridophores: without iridophores). (A) Heterozygous carriers of *alx4a*$^{ex1+8}$ were intercrossed and produced 8 progeny with iridophores and 2 progeny without. This cross follows expectations of Mendelian inheritance. χ^2= 0.058, p=0.809. (B) Presumptive carriers of *alx4a*$^{ex1-4}$ were intercrossed and produced 18 progeny with iridophores and 5 progeny without. This cross also follows expectations of Mendelian inheritance. χ^2= 0.130, p=0.718. (C) A cross between heterozygous carriers of *alx4a*$^{ex1+8}$ and *alx4a*$^{ex1-4}$ produced 49 progeny with iridophores and 17 progeny without. This cross also follows Mendelian inheritance. χ^2= 0.020, p=0.888. For all Chi square analyses, α=0.05.

Figure 9: *alx4a* mutant phenotype persists into adulthood.

Wild-type fish (top) have horizontal tripes comprised of melanophores (white arrowheads) and iridophores (blue arrowheads). *alx4a* homozygous mutants (bottom) retain the iridophore-deficient phenotype into adulthood.

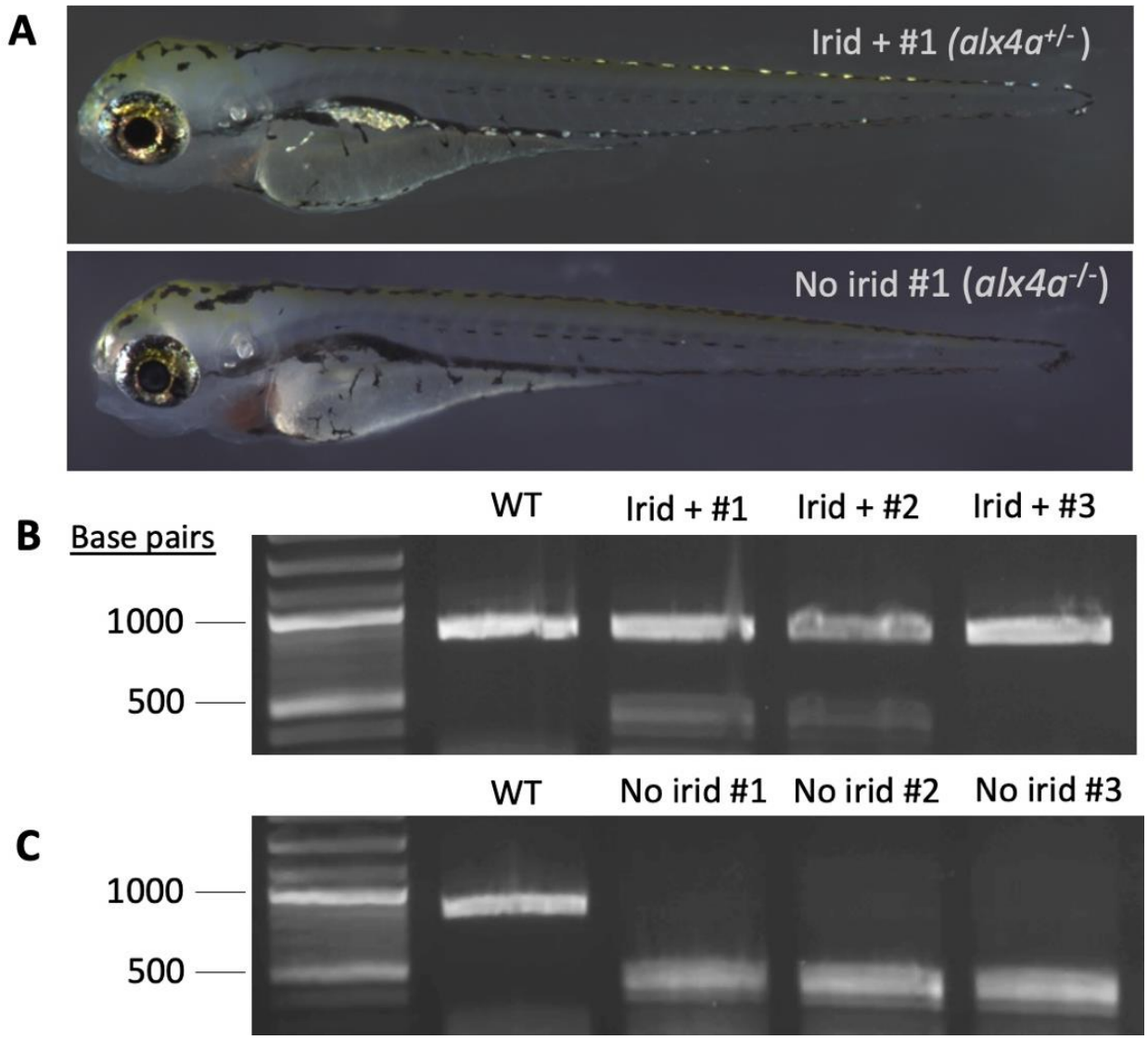

Figure 10: Confirming genotype of iridophore deficient individuals with restriction enzyme Hpy188i

(A) A larva with iridophores and a larva without iridophores and (B-C) Hppy188i restriction digest confirming genotypes. A 1076 bp band was amplified by PCR and they digested with Hppy188i. Digestion of the wild-type allele produces two bands (864 bp and 270 bp). Digestion of mutant allele produces three bands (460 bp, 412 bp, and 270 bp). In (B), lane one in the top gel is a wild-type positive control, lanes two and three show heterozygotes, and lane four shows a homozygous wild-type. In (C), lane one shows a wild-type positive control, and the next three lanes are homozygous mutants for the *alx4a* exon 1 8 bp insertion.

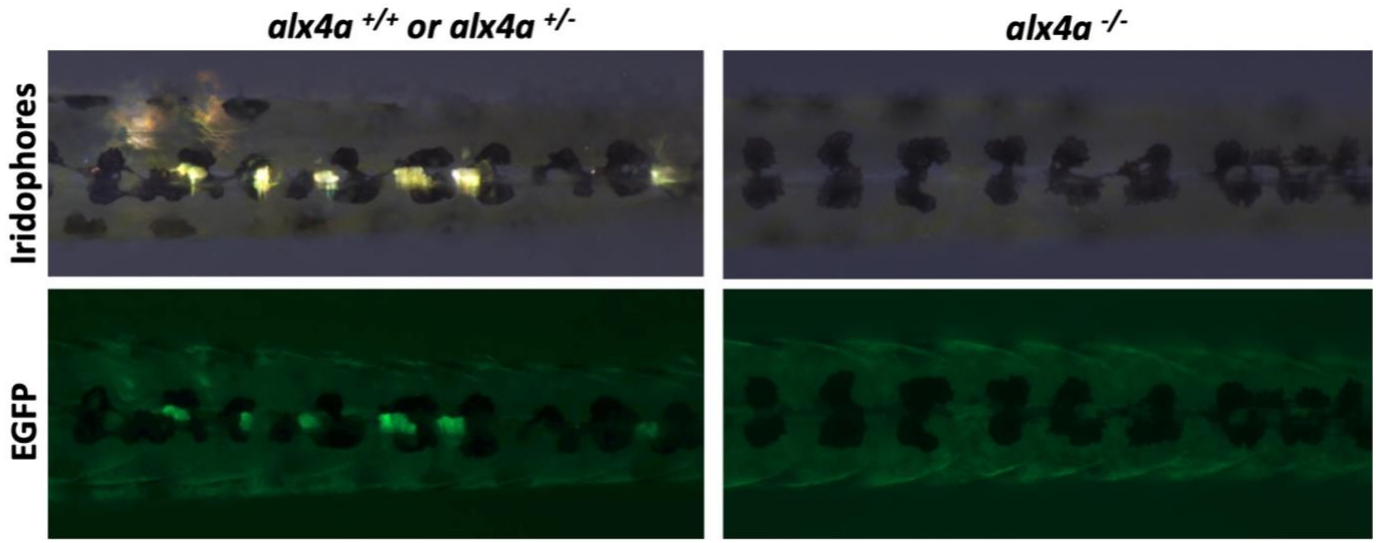

Figure 11: *alx4a*$^{-/-}$ individuals don't express iridophore marker *pnp4a*
Brightfield and fluorescent images of the dorsal stripe in 4 dpf larvae. Iridophores are present in *alx4a*$^{+/+}$ and *alx4a* $^{+/-}$ but absent in *alx4a*$^{-/-}$. Consistent with the brightfield imaging, *pnp4a:egfp* expression is seen in fish with iridophores but is missing from *alx4a*$^{-/-}$ individuals.

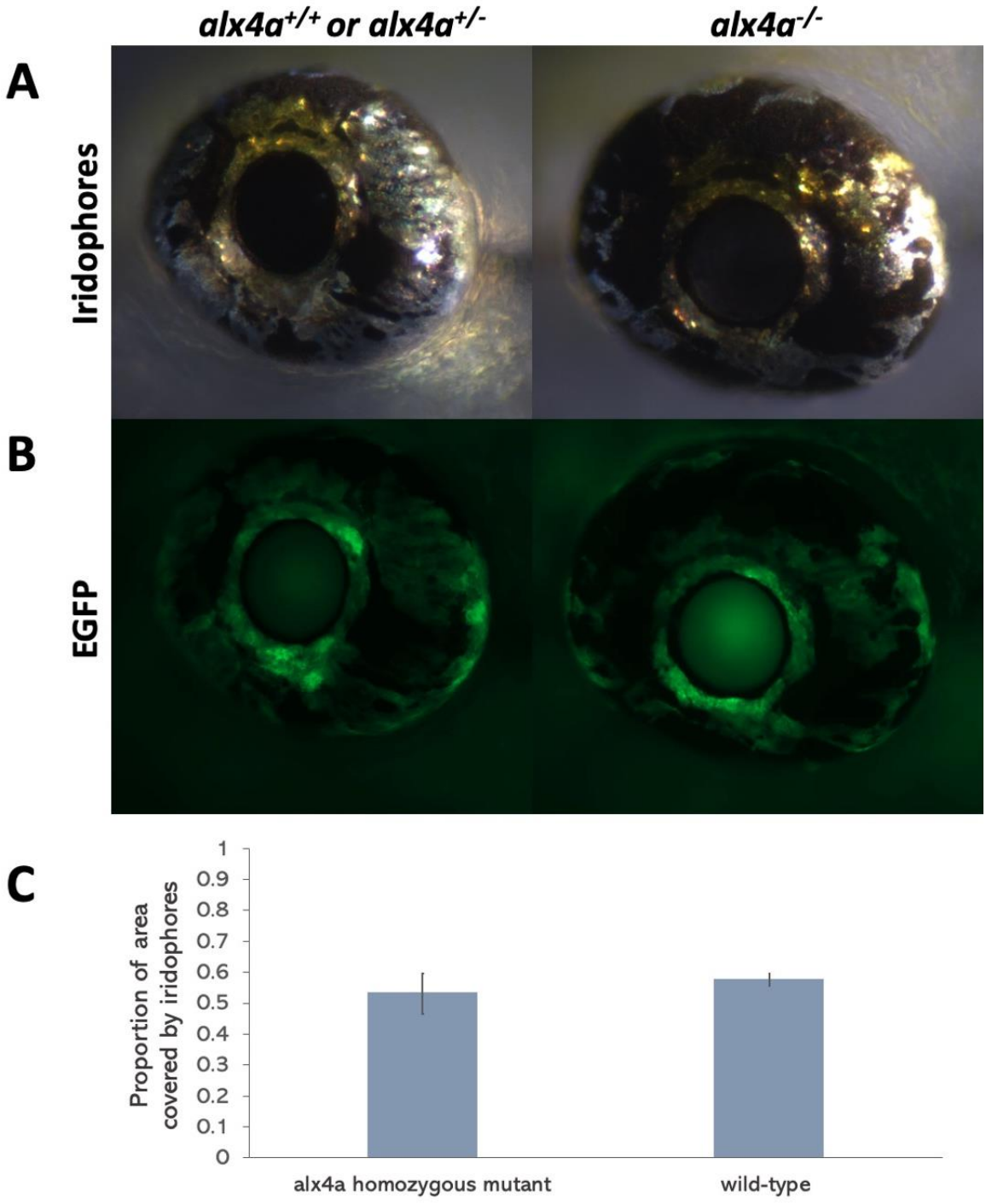

Figure 12: Retinal pigment epithelium iridophores develop independently of the body iridophores
Brightfield and fluorescent images of the retinal pigment epithelium. Both the wild-type and mutants have retinal iridophores.

AKNOWLEDGEMENTS

Research reported in this thesis was supported in part by the Rhode Island Institutional Development Award (IDeA) Network of Biomedical Research Excellence from the National Institute of General Medical Sciences of the National Institutes of Health under grant number P20GM103430.

Thank you to Dr. Larissa Patterson for introducing me to the wonderful world of research and also for patiently teaching me all of the research skills that I know.

REFERENCES

Buckingham M. 2017. Gene regulatory networks and cell lineages that underlie the formation of skeletal muscle. PNAS. 114(23):5830–5837. doi:10.1073/pnas.1610605114.

Burstyn-Cohen T, Stanleigh J, Sela-Donenfeld D, Kalcheim C. 2004. Canonical Wnt activity regulates trunk neural crest delamination linking BMP/noggin signaling with G1/S transition. Development. 131(21):5327–5339. doi:10.1242/dev.01424.

Calloni GW, Douarin NML, Dupin E. 2009. High frequency of cephalic neural crest cells shows coexistence of neurogenic, melanogenic, and osteogenic differentiation capacities. PNAS. 106(22):8947–8952. doi:10.1073/pnas.0903780106.

Cano A, Pérez-Moreno MA, Rodrigo I, Locascio A, Blanco MJ, del Barrio MG, Portillo F, Nieto MA. 2000. The transcription factor Snail controls epithelial–mesenchymal transitions by repressing E-cadherin expression. Nature Cell Biology. 2(2):76–83. doi:10.1038/35000025.

Cong L, Ran FA, Cox D, Lin S, Barretto R, Habib N, Hsu PD, Wu X, Jiang W, Marraffini LA, et al. 2013. Multiplex Genome Engineering Using CRISPR/Cas Systems. Science. 339(6121):819–823. doi:10.1126/science.1231143.

Curran K, Lister JA, Kunkel GR, Prendergast A, Parichy DM, Raible DW. 2010. Interplay between Foxd3 and Mitf regulates cell fate plasticity in the zebrafish neural crest. Developmental Biology. 344(1):107–118. doi:10.1016/j.ydbio.2010.04.023.

Curran K, Raible DW, Lister JA. 2009. Foxd3 controls melanophore specification in the zebrafish neural crest by regulation of Mitf. Developmental Biology. 332(2):408–417. doi:10.1016/j.ydbio.2009.06.010.

Davidson EH, Cameron RA, Ransick A. 1998. Specification of cell fate in the sea urchin embryo: summary and some proposed mechanisms. Development. 125(17):3269–3290.

Dee CT, Szymoniuk CR, Mills PED, Takahashi T. 2013. Defective neural crest migration revealed by a Zebrafish model of Alx1-related frontonasal dysplasia. Hum Mol Genet. 22(2):239–251. doi:10.1093/hmg/dds423.

Dorsky RI, Raible DW, Moon RT. 1998. Direct regulation of nacre, a zebrafish MITF homolog required for pigment cell formation, by the Wnt pathway. :6.

Dow LE, Fisher J, O'Rourke KP, Muley A, Kastenhuber ER, Livshits G, Tschaharganeh DF, Socci ND, Lowe SW. 2015. Inducible in vivo genome editing with CRISPR-Cas9. Nature Biotechnology. 33(4):390–394. doi:10.1038/nbt.3155.

Erickson CA, Goins TL. 1995. Avian neural crest cells can migrate in the dorsolateral path only if they are specified as melanocytes. Development. 121(3):915–924.

Greenhill ER, Rocco A, Vibert L, Nikaido M, Kelsh RN. 2011. An Iterative Genetic and Dynamical Modelling Approach Identifies Novel Features of the Gene Regulatory Network Underlying Melanocyte Development. PLOS Genetics. 7(9):e1002265. doi:10.1371/journal.pgen.1002265.

Hallsson JH, Haflidadóttir BS, Schepsky A, Arnheiter H, Steingrímsson E. 2007. Evolutionary sequence comparison of the Mitf gene reveals novel conserved domains. Pigment Cell Res. 20(3):185–200. doi:10.1111/j.1600-0749.2007.00373.x.

Henion PD, Weston JA. 1997. Timing and pattern of cell fate restrictions in the neural crest lineage. Development. 124(21):4351–4359.

Hodgkinson CA, Moore KJ, Nakayama A, Steingrímsson E, Copeland NG, Jenkins NA, Arnheiter H. 1993. Mutations at the mouse microphthalmia locus are associated with defects in a gene encoding a novel basic-helix-loop-helix-zipper protein. Cell. 74(2):395–404. doi:10.1016/0092-8674(93)90429-t.

Hudson R, Taniguchi-Sidle A, Boras K, Wiggan O, Hamel PA. 1998. Alx-4, a transcriptional activator whose expression is restricted to sites of epithelial–mesenchymal interactions. Developmental Dynamics. 213(2):159–169. doi:https://doi.org/10.1002/(SICI)1097-0177(199810)213:2<159::AID-AJA1>3.0.CO;2-F.

Jinek M, Chylinski K, Fonfara I, Hauer M, Doudna JA, Charpentier E. 2012. A programmable dual-RNA-guided DNA endonuclease in adaptive bacterial immunity. Science. 337(6096):816–821. doi:10.1126/science.1225829.

Kelsh RN, Harris ML, Colanesi S, Erickson CA. 2009. Stripes and belly-spots – a review of pigment cell morphogenesis in vertebrates. Semin Cell Dev Biol. 20(1):90–104. doi:10.1016/j.semcdb.2008.10.001.

Labun K, Montague TG, Krause M, Torres Cleuren YN, Tjeldnes H, Valen E. 2019. CHOPCHOP v3: expanding the CRISPR web toolbox beyond genome editing. Nucleic Acids Research. 47(W1):W171–W174. doi:10.1093/nar/gkz365.

LaFave MC, Varshney GK, Vemulapalli M, Mullikin JC, Burgess SM. 2014. A defined zebrafish line for high-throughput genetics and genomics: NHGRI-1. Genetics. 198(1):167–170. doi:10.1534/genetics.114.166769.

Lane BM, Lister JA. 2012. Otx but Not Mitf Transcription Factors Are Required for Zebrafish Retinal Pigment Epithelium Development. PLOS ONE. 7(11):e49357. doi:10.1371/journal.pone.0049357.

Le Douarin NM. 1980. The ontogeny of the neural crest in avian embryo chimaeras. Nature. 286(5774):663–669. doi:10.1038/286663a0.

Le Douarin NM, Teillet MA. 1973. The migration of neural crest cells to the wall of the digestive tract in avian embryo. J Embryol Exp Morphol. 30(1):31–48.

Le Lièvre CS, Le Douarin NM. 1975. Mesenchymal derivatives of the neural crest: analysis of chimaeric quail and chick embryos. J Embryol Exp Morphol. 34(1):125–154.

Lopes SS, Yang X, Müller J, Carney TJ, McAdow AR, Rauch G-J, Jacoby AS, Hurst LD, Delfino-Machín M, Haffter P, et al. 2008. Leukocyte Tyrosine Kinase Functions in Pigment Cell Development. PLOS Genetics. 4(3):e1000026. doi:10.1371/journal.pgen.1000026.

Mallarino R, Henegar C, Mirasierra M, Manceau M, Schradin C, Vallejo M, Beronja S, Barsh GS, Hoekstra HE. 2016. Developmental mechanisms of stripe patterns in rodents. Nature. 539(7630):518–523. doi:10.1038/nature20109.

Martik ML, Lyons DC, McClay DR. 2016. Developmental gene regulatory networks in sea urchins and what we can learn from them. F1000Res. 5. doi:10.12688/f1000research.7381.1. [accessed 2021 Apr 9]. https://www.ncbi.nlm.nih.gov/pmc/articles/PMC4765714/.

Mazumdar A, Mazumdar M. 2002. How one becomes many: Blastoderm cellularization in Drosophila melanogaster. BioEssays. 24(11):1012–1022. doi:https://doi.org/10.1002/bies.10184.

Milet C, Monsoro-Burq AH. 2012. Neural crest induction at the neural plate border in vertebrates. Dev Biol. 366(1):22–33. doi:10.1016/j.ydbio.2012.01.013.

Nguyen M, Arnheiter H. 2000. Signaling and transcriptional regulation in early mammalian eye development: a link between FGF and MITF. Development. 127(16):3581–3591.

Nishida H, Sawada K. 2001. macho-1 encodes a localized mRNA in ascidian eggs that specifies muscle fate during embryogenesis. Nature. 409(6821):724–729. doi:10.1038/35055568.

Parichy DM, Rawls JF, Pratt SJ, Whitfield TT, Johnson SL. 1999. Zebrafish sparse corresponds to an orthologue of c-kit and is required for the morphogenesis of a subpopulation of melanocytes, but is not essential for hematopoiesis or primordial germ cell development. Development. 126(15):3425–3436.

Petratou K, Spencer SA, Kelsh RN, Lister JA. 2021. The MITF paralog tfec is required in neural crest development for fate specification of the iridophore lineage from a multipotent pigment cell progenitor. PLOS ONE. 16(1):e0244794. doi:10.1371/journal.pone.0244794.

Petratou K, Subkhankulova T, Lister JA, Rocco A, Schwetlick H, Kelsh RN. 2018. A systems biology approach uncovers the core gene regulatory network governing iridophore fate choice from the neural crest. PLOS Genetics. 14(10):e1007402. doi:10.1371/journal.pgen.1007402.

Qu S, Niswender KD, Ji Q, van der Meer R, Keeney D, Magnuson MA, Wisdom R. 1997. Polydactyly and ectopic ZPA formation in Alx-4 mutant mice. Development. 124(20):3999–4008.

Raible DW, Eisen JS. 1994. Restriction of neural crest cell fate in the trunk of the embryonic zebrafish. Development. 120(3):495–503.

Saunders LM, Mishra AK, Aman AJ, Lewis VM, Toomey MB, Packer JS, Qiu X, McFaline-Figueroa JL, Corbo JC, Trapnell C, et al. 2019. Thyroid hormone regulates distinct paths to maturation in pigment cell lineages. Elife. 8. doi:10.7554/eLife.45181.

Scarpa E, Mayor R. 2016. Collective cell migration in development. Journal of Cell Biology. 212(2):143–155. doi:10.1083/jcb.201508047.

Serbedzija GN, Fraser SE, Bronner-Fraser M. 1990. Pathways of trunk neural crest cell migration in the mouse embryo as revealed by vital dye labelling. :10.

Shah A, Davey C, Whitebirch A, Miller A, Moens C. 2015. Rapid reverse genetic screening using CRISPR in zebrafish | Nature Methods. [accessed 2021 Feb 10]. https://www.nature.com/articles/nmeth.3360.

Shtutman M, Zhurinsky J, Simcha I, Albanese C, D'Amico M, Pestell R, Ben-Ze'ev A. 1999. The cyclin D1 gene is a target of the β-catenin/LEF-1 pathway. Proc Natl Acad Sci U S A. 96(10):5522–5527.

Sizarov A, Lamers WH, Mohun TJ, Brown NA, Anderson RH, Moorman AFM. 2012. Three-dimensional and molecular analysis of the arterial pole of the developing human heart. J Anat. 220(4):336–349. doi:10.1111/j.1469-7580.2012.01474.x.

Spiewak JE, Bain EJ, Liu J, Kou K, Sturiale SL, Patterson LB, Diba P, Eisen JS, Braasch I, Ganz J, et al. 2018. Evolution of Endothelin signaling and diversification of adult pigment pattern in Danio fishes. PLoS Genet. 14(9). doi:10.1371/journal.pgen.1007538. [accessed 2021 Feb 8]. https://www.ncbi.nlm.nih.gov/pmc/articles/PMC6161917/.

Tachibana M, Takeda K, Nobukuni Y, Urabe K, Long JE, Meyers KA, Aaronson SA, Miki T. 1996. Ectopic expression of MITF, a gene for Waardenburg syndrome type 2, converts fibroblasts to cells with melanocyte characteristics. Nat Genet. 14(1):50–54. doi:10.1038/ng0996-50.

Theveneau E, Mayor R. 2012. Neural crest delamination and migration: From epithelium-to-mesenchyme transition to collective cell migration. Developmental Biology. 366(1):34–54. doi:10.1016/j.ydbio.2011.12.041.

Tomer R, Khairy K, Amat F, Keller PJ. 2012. Quantitative high-speed imaging of entire developing embryos with simultaneous multiview light-sheet microscopy. Nat Methods. 9(7):755–763. doi:10.1038/nmeth.2062.

Whittaker JR. 1973. Segregation during ascidian embryogenesis of egg cytoplasmic information for tissue-specific enzyme development. Proc Natl Acad Sci U S A. 70(7):2096–2100. doi:10.1073/pnas.70.7.2096.

Williams JS, Hsu JY, Rossi CC, Artinger KB. 2018. Requirement of zebrafish pcdh10a and pcdh10b in melanocyte precursor migration. Developmental Biology. 444:S274–S286. doi:10.1016/j.ydbio.2018.03.022.

Xing L, Quist TS, Stevenson TJ, Dahlem TJ, Bonkowsky JL. 2014. Rapid and Efficient Zebrafish Genotyping Using PCR with High-resolution Melt Analysis. J Vis Exp.(84). doi:10.3791/51138. [accessed 2021 Mar 20]. https://www.ncbi.nlm.nih.gov/pmc/articles/PMC4116811/.

Zabierowski SE, Baubet V, Himes B, Li L, Fukunaga-Kalabis M, Patel S, McDaid R, Guerra M, Gimotty P, Dahamne N, et al. 2011. Direct reprogramming of melanocytes to neural crest stem-like cells by one defined factor. Stem Cells. 29(11):1752–1762. doi:10.1002/stem.740.

Zhao Q, Behringer RR, de Crombrugghe B. 1996. Prenatal folic acid treatment suppresses acrania and meroanencephaly in mice mutant for the Cart1 homeobox gene. Nat Genet. 13(3):275–283. doi:10.1038/ng0796-275.